

ON A 1/2-EQUATION MODEL OF TURBULENCE

RUI FANG*, WEI-WEI HAN, AND WILLIAM J LAYTON

Abstract. In 1-equation URANS models of turbulence, the eddy viscosity is given by $\nu_T = 0.55l(x,t)\sqrt{k(x,t)}$. The length scale l must be pre-specified and $k(x,t)$ is determined by solving a nonlinear partial differential equation. We show that in interesting cases the spacial mean of $k(x,t)$ satisfies a simple ordinary differential equation. Using its solution in ν_T results in a 1/2-equation model. This model has attractive analytic properties. Further, in comparative tests in 2d and 3d the velocity statistics produced by the 1/2-equation model are comparable to those of the full 1-equation model.

Key words. Turbulence, eddy viscosity model, and 1-equation model.

1. Introduction

Unsteady Reynolds-averaged Navier-Stokes (URANS) models can be developed in several ways. Here we adopt finite time averaging that does not require assumptions of ergodicity. Other approaches, leading to the same models, are common, e.g. Wilcox [34], Mohammadi and Pironneau [24], Chacon-Rebollo and Lewandowski [6]. URANS models can be viewed as approximating time averages

$$(1) \quad \bar{u}(x,t) := \frac{1}{\tau} \int_{t-\tau}^t u(x,t') dt' \text{ with fluctuation } u'(x,t) := (u - \bar{u})(x,t)$$

of solutions of the Navier-Stokes equations (NSE)

$$(2) \quad \nabla \cdot u = 0, u_t + u \cdot \nabla u - \nu \Delta u + \nabla p = f(x,t),$$

with the domain, kinematic viscosity, and initial and boundary conditions (BC-s) specified. There are a variety, 0-equation, 1-equation, 2-equation, and more-equation, of useful URANS models with (generally) increasing predictive ability as model complexity (e.g., number of equations and calibration parameters) increases. This report studies the extent flow statistics predicted by 1-equation models can be captured by a 1/2-equation model (derived in Section 2) which has 0-equation complexity.

The standard URANS approach is to model $\bar{u}(x,t)$ by eddy viscosity

$$v_t + v \cdot \nabla v - \nabla \cdot ([2\nu + \nu_T] \nabla^s v) + \nabla q = \frac{1}{\tau} \int_{t-\tau}^t f(x,t') dt', \text{ and } \nabla \cdot v = 0.$$

Here $\nu_T = 0.55l\sqrt{k}$ is the eddy viscosity. The model representation of the turbulence length scale $l(x,t)$ and turbulent kinetic energy (TKE) $k(x,t) \simeq \frac{1}{2} \overline{|u'(x,t)|^2}$ must be specified. In Section 2 we show that with kinematic $l = \sqrt{2k\tau}$ the time evolution of the space-average of $k(x,t)$

$$k(t) = \frac{1}{|\Omega|} \int_{\Omega} k(x,t) dx \simeq \frac{1}{|\Omega|} \int_{\Omega} \frac{1}{2} \overline{|u'(x,t)|^2} dx.$$

Received by the editors on March 31, 2024 and, accepted on October 10, 2024.

2000 *Mathematics Subject Classification.* 35R35, 49J40, 60G40.

*Corresponding author.

can be captured by a single ordinary differential equation (ODE) in time

$$(3) \quad \frac{d}{dt}k(t) + \frac{\sqrt{2}}{2}\tau^{-1}k(t) = \frac{1}{|\Omega|} \int_{\Omega} \nu_T |\nabla^s v|^2 dx.$$

Using $k(t)$ rather than $k(x, t)$ in ν_T reduces model complexity to that of a 0-equation model. Section 2.3 proves the positivity of $k(t)$ and the boundedness of the 1/2-equation model's kinetic energy and energy dissipation rate. Proposition 1 in Section 2.3 shows that when the time window τ is sufficiently small $k(t) \rightarrow 0$ (and thus ν_T also) reducing the model to the NSE. The other natural limit is whether the model solution converges to a Reynolds-averaged Navier-Stokes (RANS) approximation as $\tau \rightarrow \infty$. Analysis of this question is an open problem but our preliminary, heuristic analysis suggests it does hold.

The goal of URANS simulations is to give acceptable accuracy at a modest cost. One requirement for this is that the model's eddy viscosity does not over-dissipate. In Theorem 1, Section 2 we prove that for τ smaller than a specific value the model's time-averaged energy dissipation rate ϵ_{model} is bounded by the $\mathcal{O}(U^3/L)$ energy input rate

$$\limsup_{T \rightarrow \infty} \frac{1}{T} \int_0^T \epsilon_{model}(t) dt \lesssim (1 + \mathcal{R}e^{-1}) \frac{U^3}{L}.$$

This proof of non-over dissipation is given for turbulence in a box in Section 2.4. Section 3 directly addresses accuracy, comparing 1/2-equation model velocity statistics with those of 1-equation models. Since simulations of the 1/2-equation model have reduced complexity compared to 1-equation models, the tests in Section 3 indicate that the 1/2-equation model's comparable accuracy makes it worthy of further study.

Related work. Finite time averaging (1) is one of the various averages, surveyed by Denaro [9], used to develop URANS models. We select it because it is analytically coherent and computationally feasible. The equation (3) is derived by space averaging the TKE equation developed by Prandtl [28] and Kolmogorov [21]. The equation for the spaced average TKE has the simpler form (3) due to the kinematic turbulence length $l = \sqrt{2k\tau}$, Section 2.2. This $l(x, t)$ was mentioned by Prandtl, Section 2.1, but developed much later. Our previous work [19], [20], [22] has found it to be effective when boundary layers are not primary and it has been used successfully by Teixeira and Cheinet [32], [33] in geophysical fluid dynamics (GFD) simulations. Our approach to 1/2-equation models is inspired by the pioneering work of Johnson and King [17], see also Wilcox [34] Section 3.7, Johnson [16]. This work captured variations of model parameters along a body or channel by deriving and solving an ODE in x , the streamwise direction. We also note that (1) means that there is not a sharp separation between our approach to URANS herein and time-filtered large eddy simulation (LES), reviewed in Pruettt [30].

The analysis of energy dissipation rates in Section 2 builds on the important, fundamental, and compelling analysis of Doering and Foias [11] and Constantin and Doering [10]. A common failure mode of eddy viscosity models is over-dissipation (even predicting a laminar solution). Thus energy dissipation analysis, inspired by [11, 10], directly addresses the practical issues of turbulence modeling, e.g. [19, 20, 23].

2. The 1/2-equation model

The 1-equation model is reviewed in Section 2.1 followed by the derivation of the 1/2-equation model studied herein in Section 2.2. Analytical properties of the

model are developed in Sections 2.3 and 2.4. Hereafter, we will redefine the body force to simplify notation, replacing $\frac{1}{\tau} \int_{t-\tau}^t f(x, t') dt'$ by $f(x, t)$.

2.1. Background on 1-equation models. Averaging the incompressible NSE (2) by (1) leads to the exact but non-closed equations for \bar{u} :

$$\begin{aligned} \nabla \cdot \bar{u} = 0, \bar{u}_t + \bar{u} \cdot \nabla \bar{u} - \nu \Delta \bar{u} + \nabla \bar{p} + \nabla \cdot R(u, u) &= f(x, t), \\ \text{where } R(u, u) &:= \overline{u \otimes u} - \bar{u} \otimes \bar{u}. \end{aligned}$$

With few exceptions, URANS models are based on the Boussinesq assumption (that the action of $R(u, u)$ on \bar{u} is dissipative, [5]) and the eddy viscosity hypothesis (that this dissipation can be represented by an enhanced viscosity ν_T , [15]). These yield the model for $v \simeq \bar{u}$,

$$(4) \quad \nabla \cdot v = 0, v_t + v \cdot \nabla v - \nu \Delta v - \nabla \cdot (\nu_T \nabla^s v) + \nabla q = f(x, t),$$

where q is a pressure and $\nabla^s v$ is the symmetric part of the gradient tensor. Computational experience (now with rigorous mathematical support [19], [20]) is that the near wall behavior $R(u, u) = \mathcal{O}([\text{wall distance}]^2)$ must be replicated in ν_T to preclude model over-dissipation. The turbulent viscosity ν_T is an expression of the observed increase of mixing with “*the intensity of the whirling agitation*”, [31], [5], [8], p. 235. This results in the dimensionally consistent, Prandtl-Kolmogorov formula

$$\begin{aligned} \nu_T &= 0.55l\sqrt{k}, \text{ where } l(x, t) = \text{turbulence length scale,} \\ k(x, t) &\simeq \frac{1}{2} \overline{|u'(x, t)|^2} = \text{turbulent kinetic energy.} \end{aligned}$$

0-equation models specify l and relate k back to local changes in $v(x, t)$. For example, the Baldwin-Lomax [3] model uses $k(x, t) \simeq l^2 |\nabla \times v(x, t)|^2$. *2-3-...URANS models* solve the k-equation below for $k(x, t)$. Then they determine $l(x, t)$ indirectly through the solution of added nonlinear partial differential equations (PDEs) for dimensionally related turbulent flow statistics.

1-equation models, with the notable exception of the Spalart-Alamaras model, specify l and solve the associated nonlinear PDE for $k(x, t)$

$$k_t + v \cdot \nabla k - \nabla \cdot (\nu_T \nabla k) + \frac{1}{l} k \sqrt{k} = \nu_T |\nabla^s v|^2.$$

This is derived by plausible closures of an exact equation for $\frac{1}{2} \overline{|u'|^2}$, [6] p. 99, Section 4.4, [7], [24] p. 60, Section 5.3 or [26] p. 369, Section 10.3. Prandtl gave two descriptions of the physical meaning of $l(x, t)$, e.g. [28], [32]. The first is that $l(x, t)$ is an average distance turbulent eddies must go to interact. Walls constrain this distance, leading to $l = \kappa y$, where κ is the von Karman constant, Prandtl [27], and y is the wall-normal distance. The second, kinematic, specification is the distance a fluctuating turbulent eddy travels in 1 time unit. Their rate is $|u'| \simeq \sqrt{2k(x, t)}$ leading to a kinematic length scale of

$$(\text{Kinematic } l(x, t)) \quad l(x, t) = \sqrt{2k(x, t)} \tau, \quad \tau = \text{time scale of (1).}$$

This is the choice herein and by Kolmogorov, [21] for his 2-equation model. With $l = \sqrt{2k} \tau$, the 1-equation model becomes $\nu_T = \mu \sqrt{2k} \tau$ and

$$(5) \quad \begin{cases} v_t + v \cdot \nabla v - \nabla \cdot ([2\nu + \nu_T] \nabla^s v) + \nabla q = f(x, t) \text{ and } \nabla \cdot v = 0, \\ k_t + v \cdot \nabla k - \nabla \cdot (\nu_T \nabla k) + \frac{\sqrt{2}}{2} \tau^{-1} k = \nu_T |\nabla^s v|^2, \end{cases}$$

where $\nu_T = 0.55l\sqrt{k}$ and $l = \sqrt{2k}\tau$. At $t = 0$ the velocity is initialized by $v(x, 0) = v_0(x)$. At some $t^* \geq 0$ the equation for $k(x, t)$ is initialized by $k(x, t^*) = k_0(x)$. We impose standard no-slip BCs¹ at walls: $v(x, t) = 0, k(x, t) = 0$ on $\partial\Omega$.

2.2. Derivation of the 1/2-equation model. We select the kinematic length scale $l = \sqrt{2k}\tau$ yielding $\nu_T = \sqrt{2\mu k(x, t)}\tau$ and (5). The 1/2-equation model begins with the space average of the k-equation in (5). Let

$$k(t) := \frac{1}{|\Omega|} \int_{\Omega} k(x, t) dx \text{ and } \varepsilon(t) := \frac{1}{|\Omega|} \int_{\Omega} \nu_T |\nabla^s v|^2 dx.$$

Averaging the k-equation over Ω gives

$$\frac{d}{dt} \frac{1}{|\Omega|} \int_{\Omega} k dx + \frac{1}{|\Omega|} \int_{\Omega} \nabla \cdot (vk) - \nabla \cdot (\nu_T \nabla k) dx + \frac{\sqrt{2}}{2} \tau^{-1} \frac{1}{|\Omega|} \int_{\Omega} k dx = \varepsilon(t)$$

The second and third terms vanish since $k(x, t) = 0$ on $\partial\Omega$:

$$(6) \quad \begin{cases} \int_{\Omega} \nabla \cdot (vk) dx = \int_{\partial\Omega} (v \cdot n) k d\sigma = 0, \\ \int_{\Omega} \nabla \cdot (\nu_T \nabla k) dx = \int_{\partial\Omega} \nu_T \nabla k \cdot n d\sigma = 0. \end{cases}$$

In more detail, both integrals are zero for internal flows ($v = 0$ and $k = 0$ on $\partial\Omega$), shear flows ($v \cdot n = 0$ and $k = 0$ on $\partial\Omega$) and under periodic BCs. For these 3 cases, $k(t)$ satisfies exactly

$$(7) \quad \frac{d}{dt} k(t) + \frac{\sqrt{2}}{2} \tau^{-1} k(t) = \varepsilon(t) \text{ with } k(t^*) \neq 0 \text{ given.}$$

One further model refinement is needed near walls. With $k = k(t)$, $\nu_T = \sqrt{2\mu k(t)}\tau$ does not vanish at walls. Recall $y = \text{wall normal distance}$ and $\kappa = \text{von Karman-like constant}$. Since ν_T should replicate the $\mathcal{O}(y^2)$ near wall asymptotics of $R(u, u)$, we adjust ν_T at walls with a multiplier $(\kappa y/L)^2$. We thus have the 1/2-equation model

$$\begin{aligned} \nu_T &= \sqrt{2\mu k(t)}\tau \text{ for periodic boundaries,} \\ \nu_T &= \sqrt{2\mu k(t)} \left(\kappa \frac{y}{L} \right)^2 \tau \text{ for no-slip and shear boundaries,} \\ v_t + v \cdot \nabla v - \nabla \cdot ([2\nu + \nu_T] \nabla^s v) + \nabla q &= f(x, t) \text{ and } \nabla \cdot v = 0, \\ (8) \quad \frac{d}{dt} k(t) + \frac{\sqrt{2}}{2} \tau^{-1} k(t) &= \varepsilon(t). \end{aligned}$$

Remark 1. *Channel flows have walls but also inflow and outflow boundaries. Outflow BCs are non-physical and selected to do minimal harm to the upstream approximation. Inflow values for $v(x, t), k(x, t)$ are needed and must be specified from measurements*

$$v \cdot n = v_{IN}, v \cdot \tau = 0, k = k_{IN} \text{ on inflow boundary } \Gamma_{IN}.$$

With these known the volume-averaged inflow part of the convection integral is calculable:

$$\frac{1}{|\Omega|} \int_{\partial\Omega} (v \cdot n) k d\sigma = \frac{1}{|\Omega|} \int_{\Gamma_{IN}} v_{IN} k_{IN} d\sigma + \text{outflow integral.}$$

The volume-averaged diffusion integral becomes $\int_{\Gamma_{IN}} k_{IN}(x) \nabla k \cdot n d\sigma$ and is not exactly calculable due to ∇k being unknown on Γ_{IN} . When diffusion of TKE across

¹When $\nu_T = \mathcal{O}([\text{wall distance}]^2)$ there is a serious analytical question in Muckenhoupt theory [36, 35], see Amrouche, Leloup and Lewandowski [37] for interesting recent developments about the meaning of traces of $k(x, t)$ on the domain boundary. This technically difficult question does not arise for the 1/2-equation model.

the inflow boundary is much smaller than convection (a plausible but untested hypothesis), the second integral is negligible. Under these conditions the 1/2-equation model for channel flow is

$$\frac{d}{dt}k(t) + \frac{\sqrt{2}}{2}\tau^{-1}k(t) = \varepsilon(t) - \frac{1}{|\Omega|} \int_{\Gamma_{IN}} u_{IN} k_{IN} d\sigma - \text{outflow integral}.$$

Remark 2 (URANS not RANS). *RANS models aim at approximating a turbulent flow at statistical equilibrium through (via an ergodic assumption) closure of an infinite time average of the NSE. The approach to replacing $k(x, t)$ with $k(t)$ means that the model so derived is essentially a URANS model not a RANS model. Nevertheless, one can ask what happens for flows at statistical equilibrium. At statistical equilibrium, and under periodic BCs $k(t)$ approximately satisfies*

$$\frac{\sqrt{2}}{2}\tau^{-1}k(t) \simeq \frac{1}{|\Omega|} \int_{\Omega} \sqrt{2}\mu k(t)\tau|\nabla^s v|^2 dx,$$

and $k(t)$ can be approximately canceled from the equation. However, implicit k dependence remains since $v = v(x, t; k)$. At statistical equilibrium the value of k is thus (approximately) determined by

$$\begin{aligned} &\text{solve for } k: && \frac{1}{|\Omega|} \int_{\Omega} |\nabla^s v(x, t; k)|^2 dx \simeq \frac{1}{2\mu}\tau^{-2} \\ &\text{subject to: } \left\{ \begin{array}{l} v_t + v \cdot \nabla v - \nabla \cdot ([2\nu + \sqrt{2}\mu k\tau] \nabla^s v) + \nabla q = f(x), \\ \nabla \cdot v = 0. \end{array} \right. \end{aligned}$$

2.3. 1/2-equation model: basic estimates. We assume here that under periodic or no-slip BCs the model (8) has a solution that is smooth enough for standard energy estimates. While proving this for the continuum model is an open problem, existence certainly holds for its finite element method (FEM) discretization. We establish positivity of $k(t)$ and model convergence to the NSE for small τ . Analysis of model behavior for $\tau \rightarrow \infty$ is an open problem.

Proposition 1. *Consider the model (8) under no-slip or periodic boundary conditions. The following hold:*

Positivity: *If $k(t^*) > 0$ then $k(t) > 0$ for all $t \geq t^*$.*

Model convergence to NSE: *There is a $\tau_0 = \tau_0(\text{data}) > 0$ such that for $\tau < \tau_0$, $k(t) \rightarrow 0$ and $\nu_T \rightarrow 0$ exponentially in t .*

Proof. The k -equation can be rewritten as

$$\frac{d}{dt}k(t) + a(t)k(t) = 0, \text{ where}$$

$$a(t) = \frac{\sqrt{2}}{2}\tau^{-1} - \tau \frac{\mu}{L^2} \frac{1}{|\Omega|} \int_{\Omega} y^2 |\nabla^s v(x, t)|^2 dx, \quad \text{and} \quad A(t) = \int_0^t a(t') dt'.$$

Thus, $\int_{\Omega} |\nabla^s v|^2 dx \in L^1(0, T)$ implies $k(t) \geq 0$ for $0 \leq t \leq T$ because then $A(t) \in L^\infty(0, T)$ and $k(t) = \exp(-[A(t) - A(t^*)])k(t^*)$. Next, note that if $k(t) \geq 0$ for $0 \leq t \leq T$, $\nu_T \geq 0$ and the eddy viscosity term can be dropped in the standard energy estimate for the momentum equation, implying $\int_{\Omega} |\nabla^s v|^2 dx \in L^1(0, T)$. To combine these two observations and show $k(t) > 0$, suppose $\nu_T = \sqrt{2}\mu|k|\tau$. Then the two observations imply $|k(t)| = k(t)$ so $k(t) > 0$. When $A(t) > 0$, which occurs for $\tau < \tau_0$, $k(t)$ decays as claimed, completing the proof. \square

Remark 3. *Since $|y/L| \leq 1$, it suffices to take*

$$\tau_0 = 2^{-1/4} \left[\frac{1}{T} \int_0^T \left(\frac{1}{|\Omega|} \int_{\Omega} |\nabla^s v|^2 dx \right) dt \right]^{-1/2}.$$

The quantity in brackets is bounded by data uniformly in T .

Next, we establish an energy equality suggested by the NSE's kinetic energy balance, rewritten in terms of $\int \frac{1}{2}|\bar{u}|^2 + \frac{1}{2}|u'|^2 dx$, and associated á priori bounds on kinetic energy and energy dissipation.

Proposition 2. *Consider the model (8) under no-slip or periodic BCs. Sufficiently regular model solutions satisfy the energy equality*

$$(9) \quad \frac{d}{dt} \left[\frac{1}{|\Omega|} \int_{\Omega} \frac{1}{2}|v(x,t)|^2 dx + k(t) \right] + \left[\frac{1}{|\Omega|} \int_{\Omega} \nu |\nabla^s v(x,t)|^2 dx + \frac{\sqrt{2}}{2} \tau^{-1} k(t) \right] = \frac{1}{|\Omega|} \int_{\Omega} f(x,t) \cdot v(x,t) dx.$$

Let the initialization $k(t^*)$ be chosen so $k(t^*) > 0$. With

$$C = C(\text{data}) = C(f, u(x, 0), k(t^*), \nu, \tau) < \infty,$$

the following uniform in T bounds on energy and dissipation rates hold

$$\begin{aligned} \frac{1}{|\Omega|} \int_{\Omega} \frac{1}{2}|v(x,T)|^2 dx &\leq C, \\ \frac{1}{T} \int_0^T \left\{ \frac{1}{|\Omega|} \int_{\Omega} [\nu + \nu_T] |\nabla^s v(x,t)|^2 dx \right\} dt &\leq C, \\ \frac{1}{|\Omega|} \int_{\Omega} \frac{1}{2}|v(x,T)|^2 dx + k(T) &\leq C, \\ \frac{1}{T} \int_0^T \left\{ \frac{1}{|\Omega|} \int_{\Omega} \nu |\nabla^s v(x,t)|^2 dx + \frac{\sqrt{2}}{2} \tau^{-1} k(t) \right\} dt &\leq C. \end{aligned}$$

Proof. Take the inner product of the momentum equation with $v(x,t)$, apply the divergence theorem. This gives

$$\begin{aligned} \frac{d}{dt} \frac{1}{|\Omega|} \int_{\Omega} \frac{1}{2}|v(x,t)|^2 dx + \\ \frac{1}{|\Omega|} \int_{\Omega} [\nu + \nu_T] |\nabla^s v(x,t)|^2 dx = \frac{1}{|\Omega|} \int_{\Omega} f(x,t) \cdot v(x,t) dx. \end{aligned}$$

Since $k(t) \geq 0$, $\nu_T |\nabla^s v(x,t)|^2 \geq 0$ and the ν_T term can be dropped (for the kinetic energy bound) then reinserted (for the dissipation bound). Differential inequalities imply that, uniformly in T ,

$$\begin{aligned} \frac{1}{|\Omega|} \int_{\Omega} \frac{1}{2}|v(x,T)|^2 dx &\leq C(\text{data}) < \infty, \\ \frac{1}{T} \int_0^T \frac{1}{|\Omega|} \int_{\Omega} [\nu + \nu_T] |\nabla^s v(x,t)|^2 dx dt &\leq C(\text{data}) < \infty. \end{aligned}$$

Adding the k -equation gives

$$(10) \quad \frac{d}{dt} \left[\frac{1}{|\Omega|} \int_{\Omega} \frac{1}{2}|v(x,t)|^2 dx + k(t) \right] + \left[\frac{1}{|\Omega|} \int_{\Omega} \nu |\nabla^s v(x,t)|^2 dx + \frac{\sqrt{2}}{2} \tau^{-1} k(t) \right] = \frac{1}{|\Omega|} \int_{\Omega} f(x,t) \cdot v(x,t) dx.$$

Let $y(t)$ be the kinetic energy, $y(t) = \frac{1}{|\Omega|} \int_{\Omega} \frac{1}{2}|v|^2 dx + k(t)$. Then, using the Cauchy-Schwarz-Young and Poincaré inequalities shows $y'(t) + ay(t) \leq F$ where $a > 0$ and

$F = \|f\|_{L^\infty(0,\infty;L^2(\Omega))}$. Using an integrating factor shows $y(t) \leq C(a)F < \infty$ for all t . With the kinetic energy uniformly bounded, time average (10) over $0 \leq t \leq T$. This shows that the time average of the second bracketed term is bounded uniformly in T . Then we have

$$\frac{1}{|\Omega|} \int_{\Omega} \frac{1}{2} |v(x, T)|^2 dx + k(T) \leq C < \infty,$$

$$\frac{1}{T} \int_0^T \left\{ \frac{1}{|\Omega|} \int_{\Omega} \nu |\nabla^s v(x, t)|^2 dx + \frac{\sqrt{2}}{2} \tau^{-1} k(t) \right\} dt \leq C < \infty,$$

completing the proof. □

Remark 4. Since v models \bar{u} and k the kinetic energy in u' , the form of the energy inequality in Proposition 2 expresses compatibility of the model energy with the NSE.

One consequence is the following result on the time-averaged equilibrium of the k-equation.

Corollary 1. As $T \rightarrow \infty$ there holds

$$\frac{1}{T} \int_0^T \frac{1}{|\Omega|} \int_{\Omega} \nu_T dx dt = \frac{\mu\tau}{T} \int_0^T k(t) dt = \frac{\sqrt{2}\mu\tau^2}{T} \int_0^T \varepsilon(t) dt + \mathcal{O}\left(\frac{1}{T}\right).$$

Proof. Time averaging the k-equation gives

$$\frac{1}{T} (k(T) - k(0)) + \frac{\sqrt{2}}{2} \tau^{-1} \frac{1}{T} \int_0^T k(t) dt = \frac{1}{T} \int_0^T \varepsilon(t) dx dt.$$

The first term is $\mathcal{O}(1/T)$ due to the *á priori* bounds. Rearranging this gives the claimed result

$$\mu\tau \frac{1}{T} \int_0^T k(t) dt = \sqrt{2}\mu\tau^2 \frac{1}{T} \int_0^T \varepsilon(t) dt + \mathcal{O}\left(\frac{1}{T}\right).$$

□

2.4. Energy dissipation rate: turbulence in a box. We show next that the model does not over-dissipate body forced flow with periodic BCs, often called turbulence in a box. These estimates use the *á priori* bounds in Section 2.3 but require a small amount of extra notation.

Definition 1. The model energy dissipation rate is

$$\varepsilon_{model}(t) := \frac{1}{|\Omega|} \int_{\Omega} \nu |\nabla^s v(x, t)|^2 dx + \frac{\sqrt{2}}{2} \tau^{-1} k(t).$$

The scale of the body force F , large velocity scale U , length scale L and large scale turnover time T^* are, respectively,

$$\begin{aligned} F &:= \sqrt{\frac{1}{|\Omega|} \int_{\Omega} |f(x)|^2 dx}, \\ U &:= \sqrt{\limsup_{T \rightarrow \infty} \frac{1}{T} \int_0^T \left[\frac{1}{|\Omega|} \int_{\Omega} |v(x, t)|^2 dx \right] dt}, \\ L &:= \min \left\{ |\Omega|^{1/3}, \frac{F}{\sup_{x \in \Omega} |\nabla^s f(x)|}, \frac{F}{\sqrt{\frac{1}{|\Omega|} \int_{\Omega} |\nabla^s f(x)|^2 dx}}, \right. \\ &\quad \left. \sqrt{\frac{F}{\sqrt{\frac{1}{|\Omega|} \int_{\Omega} |\Delta f(x)|^2 dx}}} \right\}, \\ T^* &:= \frac{L}{U}. \end{aligned}$$

The large velocity scale U and length scale L are well defined due to Proposition 2.3.

Theorem 1. Consider the model (8) in 3d subject to periodic BCs and with $\nabla \cdot f(x) = 0$, $f \in H^2(\Omega) \cap W^{1, \infty}(\Omega)$, and $v_0(x) \in L^2(\Omega)$. The time-averaged energy dissipation rate of the model satisfies

$$\left[1 - \sqrt{2}\mu \left(\frac{\tau}{T^*} \right)^2 \right] \limsup_{T \rightarrow \infty} \frac{1}{T} \int_0^T \varepsilon_{\text{model}}(t) dt \leq 2(1 + \mathcal{R}e^{-1}) \frac{U^3}{L}.$$

With $\mu = 0.55$, if $\frac{\tau}{T^*} \leq 0.8$ then

$$\limsup_{T \rightarrow \infty} \frac{1}{T} \int_0^T \varepsilon_{\text{model}}(t) dt \leq 4(1 + \mathcal{R}e^{-1}) \frac{U^3}{L}.$$

Proof. Let $\phi(T)$ denote a generic, bounded, positive function with $\phi(T) \rightarrow 0$ as $T \rightarrow \infty$. Consider the energy estimate (9) above (which establishes that $\varepsilon_{\text{model}}(t)$ is defined correctly). Time averaging (9) gives

$$\begin{aligned} (11) \quad & \frac{1}{T} \left[\left(\frac{1}{|\Omega|} \int_{\Omega} \frac{1}{2} |v(x, T)|^2 dx + k(T) \right) - \left(\frac{1}{|\Omega|} \int_{\Omega} \frac{1}{2} |v(x, 0)|^2 dx + k(0) \right) \right] + \\ & \frac{1}{T} \int_0^T \varepsilon_{\text{model}}(t) dt = \frac{1}{T} \int_0^T \left[\frac{1}{|\Omega|} \int_{\Omega} f(x) \cdot v(x, t) dx \right] dt. \end{aligned}$$

From the *á priori* bounds in Proposition 2.3, the first term is $\mathcal{O}(1/T)$; the second term is the time average of $\varepsilon_{\text{model}}$. We thus have

$$\begin{aligned} (12) \quad & \frac{1}{T} \int_0^T \varepsilon_{\text{model}}(t) dt = \mathcal{O}\left(\frac{1}{T}\right) + \frac{1}{T} \int_0^T \left[\frac{1}{|\Omega|} \int_{\Omega} f(x) \cdot v(x, t) dx \right] dt \\ & \leq \mathcal{O}\left(\frac{1}{T}\right) + UF + \phi(T). \end{aligned}$$

Next take the inner product of (8) with $f(x)$, integrate by parts, use $\nabla \cdot f = 0$ and time average over $0 \leq t \leq T$. This gives

$$(13) \quad \begin{aligned} F^2 &= \frac{1}{T} \int_0^T \left(\frac{1}{|\Omega|} \int_{\Omega} [v(x, T) - v(x, 0)] \cdot f(x) dx \right) dt \\ &\quad - \frac{1}{T} \int_0^T \left(\frac{1}{|\Omega|} \int_{\Omega} v(x, t) \otimes v(x, t) : \nabla f(x) dx \right) dt + \\ &\quad \frac{1}{T} \int_0^T \left[\frac{1}{|\Omega|} \int_{\Omega} [\nu + \nu_T] \nabla^s v(x, t) : \nabla^s f(x) dx \right] dt. \end{aligned}$$

The first two terms on the right-hand side (RHS) are shared with the NSE. Standard estimates for those terms shared with the NSE from the pioneering work of Doering, Foias, and Constantin [11], [10] are $\mathcal{O}\left(\frac{1}{T}\right) + \frac{F}{L}U^2 + \phi(T)$. Consider the last term on the RHS. Application of the space-time Cauchy-Schwarz-Young inequality, with multipliers $\frac{\beta T^*}{2}$ and $\frac{1}{2\beta T^*}$ ($T^* = L/U$), to it gives, for any $0 < \beta < 1$,

$$(14) \quad \begin{aligned} &\frac{1}{T} \int_0^T \left[\frac{1}{|\Omega|} \int_{\Omega} [\nu + \nu_T] \nabla^s v(x, t) : \nabla^s f(x) dx \right] dt = \\ &= \frac{1}{T} \int_0^T \frac{1}{|\Omega|} \int_{\Omega} -\nu v : \Delta f dx dt + \frac{1}{T} \int_0^T \frac{1}{|\Omega|} \int_{\Omega} \nu_T \nabla^s v : \nabla^s f dx dt \\ &\leq \frac{\nu U F}{L^2} + \frac{\beta}{2} \frac{F}{U T} \int_0^T \varepsilon(t) dt + \frac{1}{2\beta} \frac{U F}{L^2 T} \int_0^T \frac{1}{|\Omega|} \int_{\Omega} \mu k(t) \tau dx dt + \phi(T). \end{aligned}$$

Inserting the estimate of the time average of $k(t)$ from Corollary 2.1 in (14) gives

$$\begin{aligned} &\frac{1}{T} \int_0^T \left[\frac{1}{|\Omega|} \int_{\Omega} [\nu + \nu_T] \nabla^s v(x, t) : \nabla^s f(x) dx \right] dt \leq \nu U \frac{F}{L^2} + \\ &+ \frac{\beta}{2} \frac{F}{U} \frac{1}{T} \int_0^T \varepsilon_{\text{model}}(t) dt + \frac{\sqrt{2}\mu\tau^2}{2\beta} U \frac{F}{L^2} \frac{1}{T} \int_0^T \varepsilon(t) dt + \mathcal{O}\left(\frac{1}{T}\right) + \phi(T). \end{aligned}$$

Use this and the previously derived, $\mathcal{O}\left(\frac{1}{T}\right) + \frac{F}{L}U^2 + \phi(T)$, estimates for the RHS terms in the equation for F^2 (13). This gives, for any $0 < \beta < 1$,

$$\begin{aligned} F^2 &\leq \nu U \frac{F}{L^2} + \frac{F}{L}U^2 + \frac{\beta}{2} \frac{F}{U} \frac{1}{T} \int_0^T \varepsilon_{\text{model}}(t) dt \\ &\quad + \frac{\sqrt{2}\mu\tau^2}{2\beta} U \frac{F}{L^2} \frac{1}{T} \int_0^T \varepsilon(t) dt + \mathcal{O}\left(\frac{1}{T}\right) + \phi(T). \end{aligned}$$

Therefore, we have the key inequality in estimating $\frac{1}{T} \int_0^T \varepsilon_{\text{model}}(t) dt$:

$$\begin{aligned} U F &\leq \nu \frac{U^2}{L^2} + \frac{U^3}{L} + \frac{\beta}{2} \frac{1}{T} \int_0^T \varepsilon_{\text{model}}(t) dt \\ &\quad + \frac{\sqrt{2}\mu\tau^2}{2\beta} \frac{U^2}{L^2} \frac{1}{T} \int_0^T \varepsilon(t) dt + \mathcal{O}\left(\frac{1}{T}\right) + \phi(T). \end{aligned}$$

The first term on the RHS $\nu \frac{U^2}{L^2}$ is rewritten as $\nu \frac{U^2}{L^2} = \frac{\nu}{LU} \frac{U^3}{L} = \mathcal{R}e^{-1} \frac{U^3}{L}$. Insert this on the RHS of the above and replace UF in (12) by the last bound. This yields

$$\begin{aligned} \frac{1}{T} \int_0^T \varepsilon_{\text{model}}(t) dt &\leq \frac{U^3}{L} + \mathcal{R}e^{-1} \frac{U^3}{L} + \frac{\beta}{2} \frac{1}{T} \int_0^T \varepsilon_{\text{model}}(t) dt + \\ &\quad + \frac{\sqrt{2}\mu}{2\beta} \left\{ \frac{\tau^2 U^2}{L^2} \right\} \frac{1}{T} \int_0^T \varepsilon(t) dt + \mathcal{O}\left(\frac{1}{T}\right) + \phi(T). \end{aligned}$$

The multiplier in braces $\frac{\tau^2 U^2}{L^2} = \left(\frac{\tau}{T^*}\right)^2$. Pick $\beta = 1$ and use

$$\frac{1}{T} \int_0^T \varepsilon(t) dt = \frac{1}{T} \int_0^T \frac{\sqrt{2}}{2} \tau^{-1} k(t) dt + O(1) \leq \frac{1}{T} \int_0^T \varepsilon_{\text{model}}(t) dt + \phi(T).$$

Proposition 2.3 shows that $\frac{1}{T} \int_0^T \varepsilon_{\text{model}}(t) dt$ is bounded uniformly in T . Thus its limit superior as $T \rightarrow \infty$ exists. This (plus an arithmetic calculation) completes the proof:

$$\left[1 - \sqrt{2}\mu \left(\frac{\tau}{T^*}\right)^2\right] \limsup_{T \rightarrow \infty} \frac{1}{T} \int_0^T \varepsilon_{\text{model}}(t) dt \leq 2(1 + \mathcal{R}e^{-1}) \frac{U^3}{L}.$$

□

3. Testing the 1/2-equation model

We test how close the 1/2-equation model velocity statistics are to volume-averaged velocity statistics produced by the 1-equation model with Prandtl's classical $l = 0.41y$ and with the kinematic turbulence length scale $l = \sqrt{2k(x,t)}\tau$. Since the 1/2-equation model's $k(t)$ allows temporal variations, our intuition is that a time-independent body force, leading to a flow where statistical equilibrium is expected, is a non-trivial test.

3.1. Flow statistics. Evaluation of flow statistics means comparing plots of 1d curves of aggregate velocity-based quantities. We calculate the time evolution of the four velocity statistics: the Taylor microscale (an average velocity length scale), the kinetic energy of the mean flow, enstrophy (aggregate vorticity), and the model approximation to the turbulent intensity:

$$\begin{aligned} \text{Taylor Microscale} & : \lambda_{Taylor} := \frac{1}{15} \left(\frac{\frac{1}{|\Omega|} \int_{\Omega} |\nabla^s v(x,t)|^2 dx}{\frac{1}{|\Omega|} \int_{\Omega} |v(x,t)|^2 dx} \right)^{-1/2} \\ \text{Kinetic Energy/Volume} & : E(t) := \frac{1}{|\Omega|} \int_{\Omega} \frac{1}{2} |v(x,t)|^2 dx \\ \text{Enstrophy/Volume} & : Ens(t) := \frac{1}{|\Omega|} \int_{\Omega} \frac{1}{2} |\nabla \times v(x,t)|^2 dx \\ \text{Turbulence Intensity} & : I_{\text{model}}(t) = \frac{\frac{1}{|\Omega|} \int_{\Omega} 2k(x,t) dx}{\frac{1}{|\Omega|} \int_{\Omega} 2k(x,t) + |v(x,t)|^2 dx} \end{aligned}$$

3.2. The 3d test problem. We examined the classical Taylor-Couette flow between counter-rotating cylinders with no-slip BCs. We used FEniCSx with the computational environment DOLFINx/0.5.2. We compared three models: the 1/2-equation model in Section 2.3, the 1-equation model in equation (5), and Prandtl's classical model with $l = 0.41y$, where y is the wall-normal distance. The κ multiplier in $(\kappa y/L)^2$ is a von Karman-like constant whose best values are unknown. We do not know if 0.41 is the correct calibration in the multiplier $(\kappa y/L)^2$. In the 3d test we tested $\kappa = 1$ in the multiplier $(\kappa y/L)^2 = (y/L)^2$. We used the backward Euler time discretization for both the momentum and k-equation plus a time filter from [13] for the momentum equation to increase time accuracy and anti-diffuse the implicit method. We used the Taylor-Hood ($P2 - P1$) element pair for the momentum equation in all cases. For the 1-equation model simulations, we used $P1$ Lagrange elements for the k-equation. The unstructured mesh was generated with GMSH, with GMSH target mesh size parameter $lc = 0.04$. The domain is given by

$$\Omega = \{(x, y, z) : r_{inner}^2 \leq x^2 + y^2 \leq r_{outer}^2, 0 \leq z \leq z_{max}\},$$

with $r_{inner} = 0.833$ and $r_{outer} = 1$ and $z_{max} = 2.2$, see Figures 1 and 2. Periodic BCs were imposed in the z direction. The outer cylinder remained stationary, while the inner cylinder rotation drove the flow. The angular velocity of the inner

cylinder, ω_{inner} , started at 0 at $t = 0$ and gradually increased until fully turned on with $\omega_{inner} = 9$ at time $t = 5$. We chose the final time $T = 30$. The time scale was set to be $\tau = 0.1$, and timestep $\Delta t = 10^{-2}$. We set $\nu = 10^{-3}$, took $U =$ inner cylinder speed and $L = 1.0 - 0.833 = 0.167$, the cylinder gap, yielding $\mathcal{R}e = 1.5 \times 10^3$. The radius ratio η and Taylor number Ta are

$$\eta := \frac{r_{inner}}{r_{outer}} = 0.833 \text{ and } Ta := 4\mathcal{R}e^2 \frac{1-\eta}{1+\eta} \simeq 8 \times 10^5.$$

Figure 1, p. 156 in [1] (see also [12]) indicates the physical flow is expected to have turbulent Taylor cells for these parameters.



FIGURE 1. The domain Ω .

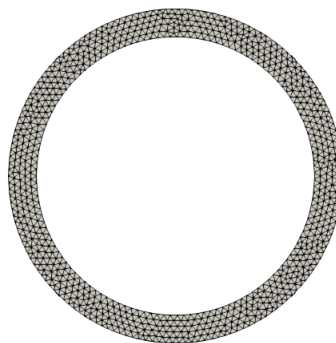


FIGURE 2. The mesh viewed from the top.

3.2.1. 3d Statistical result analysis. We first compared the 1/2-equation velocity to both 1-equation velocities. All 3 models gave a time-averaged kinetic energy (to 2 digits) of 3.6. The L^2 norms of time-averaged differences $\|v_{1/2eqn} - v_{1eqn}\|$, $\|v_{1/2eqn} - v_{1eqn\&l=\kappa y}\|$ were (to 2 digits) 0.17 and 0.14 respectively. (These norms were calculated using nodal values in a standard way and are known in finite element theory [4] to be equivalent to the continuous L^2 norms.) This yielded a percent difference of respectively 4.7% and 3.9%, in Figure 3:

$$\frac{\|v_{1/2eqn} - v_{1eqn}\|_{L^2}}{\|v_{1eqn}\|_{L^2}} \simeq 0.047 \text{ and } \frac{\|v_{1/2eqn} - v_{1eqn\&l=\kappa y}\|_{L^2}}{\|v_{1eqn\&l=\kappa y}\|_{L^2}} \simeq 0.039.$$

Given the 1/2-equation model parameters were non-calibrated, these velocity differences seem acceptable.

The tests did show k -value differences between the non-calibrated 1/2-equation $k(t)$ and the space average of $k(x, t)$ for the 2 models. These differences are also reflected in the computed approximations of the turbulent intensities (as these depend on the k values). In the 2d tests below a well-resolved NSE simulation is available for comparison. The 2d results suggest that here the k value of the 1-equation model is too large due to ν_T being too large in the near wall region. This suggests the 1/2-equation model results for $k(t)$ and the turbulent intensity, being closer to the model with $l = 0.41y$, are again acceptable, Figure 4, Figure 5.

The Taylor microscale λ_{Taylor} depends on velocity gradients more sensitive to model parameters and mesh than velocities. Predictions of λ_{Taylor} are very similar in all models from 10^{-3} to 1.5×10^{-3} , Figure 6. For this problem, we believe the model with $l = 0.41y$ is more accurate than the other 1-equation model due to its near-wall asymptotics being closer to that of the Reynolds stress. Thus, the 1/2-equation model's closeness to the former is another model success.

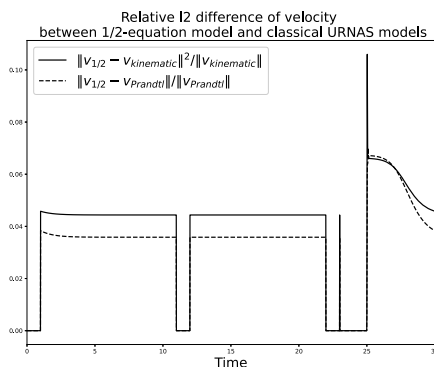


FIGURE 3. Relative error.

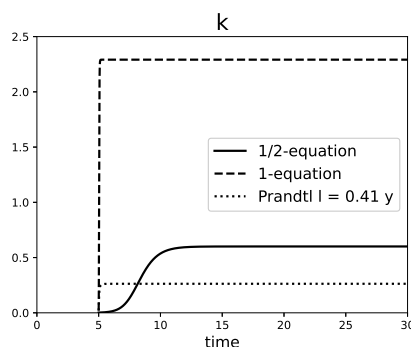


FIGURE 4. The k value.

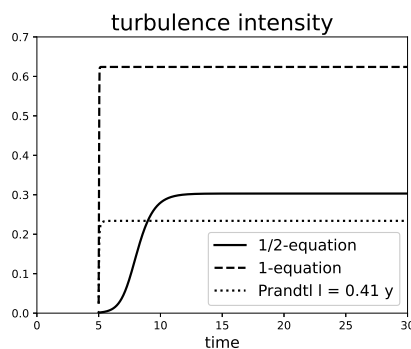


FIGURE 5. The turbulence intensity.

The enstrophy values indicate significant rotational motions. The previous results suggest the $k(x, t)$ values for the 1-equation model with $l = \sqrt{2k}\tau$ are too large for this problem. This makes ν_T too large and the model velocity over-diffused. Thus lower enstrophy is expected. In Figure 7, the 1/2-equation model has enstrophy close to the model solution with $l = \kappa y$ and above the 1-equation model with $l = \sqrt{2k}\tau$. The magnitude of velocity at time $t = 10$ for all the models

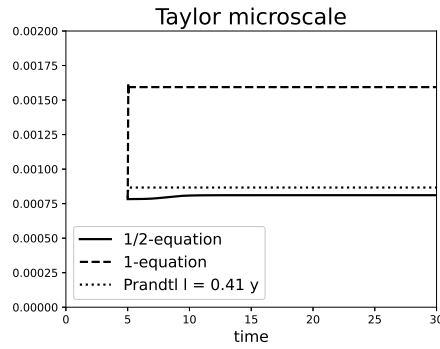


FIGURE 6. The Taylor microscale.

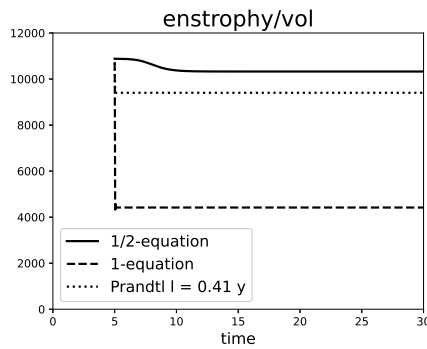


FIGURE 7. The enstrophy over volume.

is presented in Figure 8. The z components of the models' velocity are plotted in Figure 9. In these, we can see vertical rotations consistent with irregular Taylor cells.

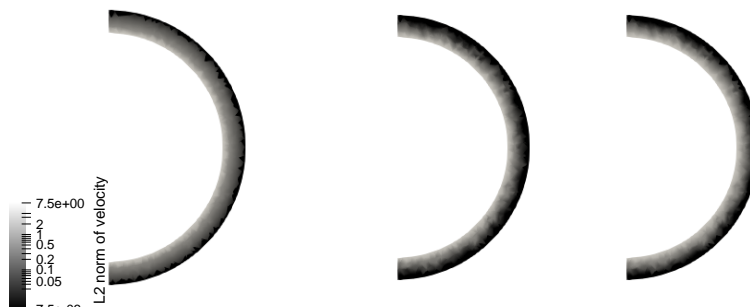


FIGURE 8. The L^2 norm of the velocity on right half of the slice $z = 1.1$ at $t = 10$ on a log scale ranging from $7.5e - 3$ to 7.5 . In the figure from left to right: classical URANS models kinetic turbulence length scale and Prandtl, and 1/2-equation model.



FIGURE 9. The velocity magnitude in the z-axis at $t = 10$ on a log scale ranging from $2.5e - 6$ to $2.5e - 2$. In the figure from left to right: classical URANS models kinetic turbulence length scale and Prandtl, and 1/2-equation model. We observe that vertical rotations are consistent with irregular Taylor cells.

3.3. The 2d test problem. Recall that κ in $l = \kappa y$ is the traditional von Karman constant with traditional value $\kappa = 0.41$. In the model, the κ in $(\kappa y/L)^2$ is a von Karman-like constant whose optimal value is not (yet) known. We test here (this κ) $\kappa = 0.41$ and test $\kappa = 1.0$ in 3d in Section 3.2. For the 2d tests of flow between offset circles, we selected $\kappa = 0.41$ in the multiplier $(\kappa y/L)^2$. Since this problem is 2d, we were able to perform a well-resolved NSE simulation for comparison. We compared the 1/2-equation model velocity statistics to the 1-equation model statistics with $\nu_T = \sqrt{2\mu k(x,t)}\tau$ and with velocity statistics computed from the well-resolved NSE simulation. The other details of the 2d tests are as follows. The computational domain is a disk with a smaller off-center obstacle inside.

$$\Omega = \{(x, y) : x^2 + y^2 \leq r_1^2 \cap (x - c_1)^2 + (y - c_2)^2 \geq r_2^2\},$$

where we set $r_1 = 1$, $r_2 = 0.1$, $c = (c_1, c_2) = (\frac{1}{2}, 0)$. No-slip BCs are imposed on both circles. The flow is driven by a counterclockwise force $f(x, y, t) = (-4y \min(t, 1)(1 - x^2 - y^2), 4x \min(t, 1)(1 - x^2 - y^2))$. We set $\tau = 0.1$, $\mu = 0.55$, $\nu = 10^{-4}$, $L = 1$, $U_{\max} = 1$ and $Re = \frac{UL}{\nu}$. The final time is $T = 15$. The k-equation is initialized at $t^* = 1$.

Initial and boundary conditions: For the 1-equation model and the 1/2-equation model, we choose initialization for the 2 k -equations as in [20]: $t^* = 1$ and

$$k(x, 1) = \frac{1}{2\tau^2} l^2(x), l(x) = \min\left\{\kappa y, 0.082Re^{-1/2}\right\}, \text{ and}$$

$$k(1) = \frac{1}{|\Omega|} \frac{1}{2\tau^2} \int_{\Omega} l(x)^2 dx.$$

The boundary condition for the k-equation is homogeneous Dirichlet.

Discretization: We employ the Taylor-Hood ($P2 - P1$) finite element pair for approximating the velocity and pressure and $P1$ Lagrange element for the TKE equation. We choose the timestep $\Delta t = 0.01$ and use the backward Euler time discretization. The mesh is generated by the Delaunay triangular method with 40 mesh points on the outer circle and 20 mesh points on the inner circle. This mesh has the longest edge $\max_e h_e = 0.208201$ and the shortest edge $\min_e h_e =$

0.0255759. For the well-resolved NSE solve, we use a finer mesh with 80 mesh points on the outer circle and 60 mesh points on the inner circle, extended by a Delaunay triangulation. This mesh has the longest edge $\max_e h_e = 0.108046$ and the shortest one $\min_e h_e = 0.0110964$. The 2d tests were performed with FreeFEM++, Hecht [14].

3.3.1. 2d Statistical result analysis. The space average of the 1-equation model's $k(x, t)$ was larger than the 1/2-equation model's $k(t)$ as in 3d. This is likely because of the difference between the sizes of the two models ν_T values near the inner disk². This led to the question of which model's velocity statistics were more accurate. For this reason, we performed the well-resolved NSE simulation.

Figures 10, 11, and 12 present the comparison of the evolution of the respective kinetic energies, enstrophy, and Taylor microscales. We observe that the kinetic energy of the 1/2-equation model is slightly less than that of the well-resolved NSE test but closely tracks its behavior. The 1-equation model's kinetic energy is incorrect. The same behavior was observed for the enstrophy and Taylor microscales in Figures 11, and 12.

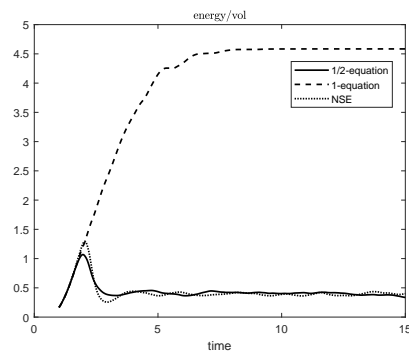


FIGURE 10. The kinetic energy over volume.

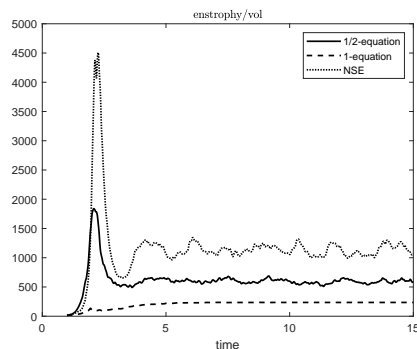


FIGURE 11. The enstrophy over volume.

²Options to correct the 1-equation model include near wall clipping [19] or rescaling [20] or damping functions [25]. These were not done because we test here the 1/2 equation model.

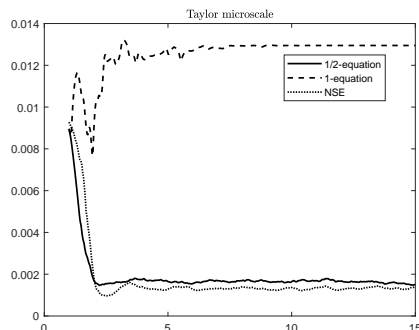


FIGURE 12. The Taylor microscale.

4. Conclusions

Due to the computational costs of Direct Numerical Simulation (DNS) and LES, RANS and URANS models are still widely used. This suggests two fruitful directions of URANS research: lowering simulation costs preserving current accuracy and raising accuracy at current simulation costs. The 1/2-equation model herein aims at the former. The model derivation, analysis, and tests indicate the 1/2-equation model is worthy of further study and the idea behind it of further development. The 1/2-equation model (8) produced velocity statistics comparable to the same velocity statistics for 1-equation models in our tests. No model is perfect so further tests delineating failure modes would be useful. The next interesting tests include flows with time-varying body forces and with interior shear layers. There are also many parallel analytical questions.

Our longer-term motivation was to use a similar idea to simplify more complex models such as 2-equation models. In these, the TKE equation is well grounded in mechanics, but the second equation, used to determine the turbulence length scale indirectly, is often a product of optimism, data fitting, and experience-informed intuition. For these a simplified model for $l(t)$ (thus a 3/2-equation model) is an interesting possibility to explore, building on work here in the most basic case.

The existence of solutions to the model (8) is a non-trivial open problem.

Acknowledgement

This research herein of William Layton and Rui Fang was supported in part by the NSF under grant DMS 2110379 and DMS 2410893. We also gratefully acknowledge the support of the University of Pittsburgh Center for Research Computing through the resources provided on the SMP cluster. The author Wei-Wei Han was partially supported by the Innovative Leading Talents Scholarship established by Xi'an Jiaotong University.

References

- [1] C.D. Andereck, S.S. Liu, S.S. and H.L. Swinney, Flow regimes in a circular Couette system with independently rotating cylinders, *Journal of Fluid Mechanics*, 164 (1986) 155-183.
- [2] F. Brossier and R. Lewandowski, Impact of the variations of the mixing length in a first order turbulent closure system, *ESAIM: Mathematical Modelling and Numerical Analysis*, 36 (2002) 345-372.
- [3] Baldwin, B.S. and Lomax, H. Thin Layer Approximation and Algebraic Model for Separated Turbulent Flows, *AIAA Paper*, 78-0257, 1978.

- [4] S.C. Brenner and L.R. Scott. *The Mathematical Theory of Finite Element Methods*, Springer-Verlag, New York, 2008.
- [5] J. Boussinesq, *Essai sur la théorie des eaux courantes*, Mémoires présentés par divers savants à l'Académie des Sciences 23 (1877): 1-680
- [6] T. Chacon-Rebollo and R. Lewandowski, *Mathematical and numerical foundations of turbulence models and applications*, Springer, New York, 2014.
- [7] P. Davidson, *Turbulence: an introduction for scientists and engineers*. Oxford Univ. Press, 2015.
- [8] O. Darrigol, *Worlds of flow*, Oxford, 2005.
- [9] F.M. Denaro, *A critical review of the Reynolds Averaged formulations for steady and unsteady turbulence. Statistical or local averaging?*, technical report, 2023.
- [10] C.R. Doering and P. Constantin, *Energy dissipation in shear driven turbulence*, *Physical Review Letters*, 69 (1992) 1648.
- [11] C. Doering and C. Foias, *Energy dissipation in body-forced turbulence*, *Journal of Fluid Mechanics*, 467 (2002) 289-306.
- [12] S. Grossmann, D. Lohse and C. Sun, *High-Reynolds number Taylor-Couette turbulence*. *Annual Review of Fluid Mechanics*, 48, (2016) 53-80.
- [13] A. Guzel and W. Layton, *Time filters increase accuracy of the fully implicit method*. *BIT Numerical Mathematics*, 58 (2018) 301-315.
- [14] F. Hecht, *New development in FreeFEM++*, *Journal of Numerical Mathematics*, 20 (2012) 251-66
- [15] Nan Jiang, W. Layton, M. McLaughlin, Yao Rong and Haiyun Zhao, *On the foundations of eddy viscosity models of turbulence*, *Fluids*, 5(2020), p. 167.
- [16] D.A. Johnson, *Transonic flow predictions with an Eddy Viscosity/Reynolds-stress closure model*, *AIAA Journal*, 25(1987) 252-259.
- [17] D.A. Johnson and L.S. King, *A mathematically simple turbulence closure model for attached and separated boundary layers*, *AIAA Journal*, 23(1985) 1684-1692.
- [18] F.T. Johnson, E.N. Tinoco and N.J. Yu, *Thirty years of development and application of CFD at Boeing Commercial Airplanes*, Seattle, *Computers & Fluids*, 34 (2005) 1115-1151.
- [19] K. Kean, W. Layton, and M. Schneier. *Clipping over dissipation in turbulence models* *International Journal of Numerical Analysis & Modeling*, 19 (2022) 424-438.
- [20] K. Kean, W. Layton, and M. Schneier, *On the Prandtl–Kolmogorov 1-equation model of turbulence*, *Philosophical Transactions of the Royal Society A*, 380 (2022) 20210054.
- [21] A.N. Kolmogorov, *Equations of turbulent motion in an incompressible fluid*, *Izv. Akad. Nauk SSSR, Seria fizichesk.*, 6 (1-2) (1942) 56-58.
- [22] W. Layton and M. McLaughlin. *On URANS Congruity with Time Averaging: Analytical laws suggest improved models*. pp. 85-108 in: : Pinelas, S., Kim, A., Vlasov, V. (eds) *Mathematical Analysis With Applications: In Honor of the 90th Birthday of Constantin Corduneanu*, Ekaterinburg, Russia, July 2018, CONCORD-90, Springer Proc. in Math. and Stat., v. 318. <https://doi.org/10.1007/978-3-030-42176-210>
- [23] W. Layton and M. Schneier. *Diagnostics for eddy viscosity models of turbulence including data-driven/neural network based parameterizations*, *Results in Applied Mathematics*, 8 (2020) 100099.
- [24] B. Mohammadi and O. Pironneau, *Analysis of the K-Epsilon Turbulence Model*, Masson, Paris, 1994.
- [25] A. Pakzad, *Damping Functions correct over-dissipation of the Smagorinsky Model*, *Mathematical Methods in the Applied Sciences*, 40 (2017) 5933-5945.
- [26] S. Pope, *Turbulent Flows*, Cambridge Univ. Press, Cambridge, 2000.
- [27] L. Prandtl, *The Mechanics of Viscous Fluids*. In: W.F., D. (ed.), *Aerodynamic Theory III*. Berlin: Springer, 1935.
- [28] L. Prandtl, *Über ein neues Formelsystem für die ausgebildete Turbulenz*, *Nachr. Akad. Wiss. Göttingen, Math-Phys. Kl.*, (1945) 6-16.
- [29] L. Prandtl, *On fully developed turbulence*, in: *Proceedings of the 2nd International Congress of Applied Mechanics*, Zurich, (1926) 62-74.
- [30] C.D. Pruett, 2008. *Temporal large-eddy simulation: theory and implementation*. *Theoretical and Computational Fluid Dynamics*, 22 (2008) 275-304.
- [31] A.J.C. Saint-Venant (Barré), *Note à joindre au Mémoire sur la dynamique des fluides*, CRAS, 17(1843) 1240-1243.

- [32] J. Teixeira and S. Cheinet, A New Mixing Length Formulation for the Eddy-Diffusivity Closure, Naval Research Laboratory Memorandum Report NRL/MR/7532-01-7244, NRL, Monterey, CA, May 2001, 25 pp.
- [33] J. Teixeira and S. Cheinet, A Simple Mixing Length Formulation for the Eddy-Diffusivity Parameterization of Dry Convection, *Boundary-Layer Meteorology* 110 (2004) 435–453.
- [34] D.C. Wilcox, *Turbulence Modeling for CFD*, DCW Industries, La Canada, 2006.
- [35] J. Scott Bradley, Hardy Inequalities with Mixed Norms, *Canadian Mathematical Bulletin*, 21 (1978) 405–408.
- [36] B. Muckenhoupt, Hardy's Inequality with Weights, *Studia Mathematica*, 44 (1972) 31–38.
- [37] C. Amrouche, G. Leloup, and R. Lewandowski, TKE Model Involving the Distance to the WallPart 1: The Relaxed Case, *Journal of Mathematical Fluid Mechanics*, 26 (2024) 58.

Department of Mathematics, University of Pittsburgh, Pittsburgh, PA 15260, USA
E-mail: `ruf10@pitt.edu`
URL: `https://ruf10.github.io`

School of Mathematics and Statistics, Xi'an Jiaotong University, Xi'an, Shaan Xi 710049, China
E-mail: `hanweiwei@stu.xjtu.edu.cn`

Department of Mathematics, University of Pittsburgh, Pittsburgh, PA 15260, USA
E-mail: `wjl@pitt.edu`